INSTITUTE OF PHYSICS PUBLISHING PLASMA PHYSICS AND CONTROLLED FUSION

Plasma Phys. Control. Fusion **45** (2003) 289–300 PII: S0741-3335(03)37820-0

Isotropic and anisotropic components of neutron emissions at the FN-II and PACO dense plasma focus devices

F Castillo[1], J J E Herrera[1], J Rangel[1], M Milanese[2,4], R Moroso[2], J Pouzo[2,4], J I Golzarri[3] and G Espinosa[3]

[1] Instituto de Ciencias Nucleares, Universidad Nacional Autónoma de México A.P. 70-543, Ciudad Universitaria, 04511, México, D.F., México
[2] Instituto de Física Arroyo Seco, Facultad de Ciencias Exactas, Universidad Nacional del Centro de la Provincia de Buenos Aires, Pinto 399, (7000) Tandil, Argentina
[3] Instituto de Física, Universidad Nacional Autónoma de México. Apdo. Postal 20-364, 01000 México, D.F. México

E-mail: herrera@nuclecu.unam.mx

Received 10 June 2002
Published 24 February 2003
Online at stacks.iop.org/PPCF/45/289

Abstract

The average angular distribution of neutron emissions has been measured in the Fuego Nuevo II (FN-II) dense plasma focus device (5 kJ) by means of CR-39 plastic nuclear track detectors. When pure deuterium is used as the filling gas, the data can be adjusted to a Gaussian function, related to anisotropic emission, superposed on a constant pedestal, related to isotropic emission. When deuterium–argon admixtures are used, the anisotropic contribution is best represented by a parabola. The same analysis is applied to previously reported results, for fewer shots, in pure deuterium from the PACO device, which is similar in size to the FN-II. In both devices the anisotropic component is smaller than the isotropic one, but with different features. In PACO the anisotropic component is concentrated on a large narrow beam around the axis, but its contribution to the total neutron yield is significantly smaller than in the FN-II, where the anisotropic component spreads over a wider range. The neutron flux per shot is monitored in both devices with calibrated silver activation detectors, at 20° and at 90° from the axis. The average values of the neutron flux at these two angles are used, along with the angular distributions obtained form the track detectors, in order to estimate the absolute neutron yield of both the isotropic and the anisotropic contributions. From examining different groups of shots, it is found that the shape of the angular distribution is important in the estimation of anisotropy, and that the value usually reported, as the ratio of neutron counts head-on and side-on, as measured by activation counters, may be misleading.

[4] Members of the Researcher Career of CONICET, Argentina.

 © 2003 IOP Publishing Ltd Printed in the UK

1. Introduction

The high neutron yield of the plasma focus machine, when filled with deuterium gas, has attracted wide attention since its development, more than three decades ago (Mather 1971, Brzosco *et al* 1997, Bernard *et al* 1998). Up to date, it is arguably the most accessible source of fusion neutrons, and research is underway in order to produce small, high repetition rate devices for applications, not only as neutron sources (Moreno *et al* 2002), but also as x-ray sources for microelectronics lithography (Lee *et al* 1998) and biomedical studies (Dubrovsky *et al* 1998). However, evidence exists, since the early days of plasma focus research, that the origin of such neutrons is not necessarily thermonuclear (Bernstein and Hai 1970, Milanese and Pouzo 1978), and the actual mechanism of neutron production in plasma foci has ever since been a source of controversy.

It has been well established that an energetic ion beam is produced in the forward direction (Jäger and Herold 1987, Rhee *et al* 1988, Moo *et al* 1991, Kelly and Márquez 1996), which results in an anisotropic neutron generation (Aliaga and Choi 1998, Castillo *et al* 1997, 2002). Although there has been considerable theoretical work on the study of the acceleration mechanisms for such ion beams, proper diagnostics that can discriminate between existing theories, are still lacking. The dynamics of the ions is rather complex during the compression phase, and the rise time of neutron signals is faster than the thermalization time. Thus, even if one surmises that thermalization might be achieved within the timescale of this phase, it is reasonable to believe that different neutron generation mechanisms coexist, yielding both isotropic and anisotropic components in the neutron emission (Castillo *et al* 2000, 2002). On the other hand, many laboratories rely on the measurements of calibrated activation counters in order to estimate the total neutron yield, but if the neutron emission is anisotropic, their results can be affected by the position of such counters. Placing counters both head-on and side-on may help to get a better picture of the neutron emission, but as we show in this work, this is not enough. It is our purpose to establish better methods to estimate the average contributions of both the isotropic and anisotropic components of the neutron angular distribution, and thus to be able to improve the estimation of the average neutron yield.

Time resolved measurements of the evolution of the neutron emission for angles between 0° and 90° from the axis, have been made by Aliaga-Rossel and Choi (1998) for a medium-size device (DPF-78, 28 kJ, 60 kV) and by Yap *et al* (1997) in a small device (3.3 kJ, 15 kV). They have shown that the head-on neutron pulse lasts longer than the side-on pulse. Furthermore, they have found that, when a doping gas is added, the anisotropy is significantly increased; the neutron pulse decays faster at larger angles, while the head-on pulse remains essentially unchanged. As the concentration of the doping gas increases, the length of the side-on pulse decreases, and a double structure in the neutron emission is revealed. If the Z of the doping gas is increased, the second peak disappears from the side-on signals. This suggests the existence of two different neutron generation mechanisms, which can be selectively affected by the doping level, as well as the Z of the doping gas. This might be related to earlier observations in larger devices, such as those at the Frascati (1 MJ) (Maisonnier *et al* 1972) and Poseidon (780 kJ, 60 kV) (Herold *et al* 1985, Jäger and Herold 1987), devices. In both these devices, neutrons were emitted in two distinct periods; the first one during the final phase of radial compression, and the second one during the expansion of the plasma column. However, it is not clear, so far, if the mechanisms responsible for the two neutron pulses in small devices are the same as those involved in large ones, since in the latter the size of the second pulse is clearly distinguished and larger than the first one. In contrast, the second pulse in medium- and small-size devices is smaller than the first one, and practically masked by it.

Although they fail to give information on the plasma dynamics, time integrated diagnostics are also useful, particularly when statistical information, such as the average neutron yield, is needed. This would be the case when applications are in mind, where a sample is subject to radiation from several shots. Plastic nuclear track detectors have played an important role in plasma focus research. They have been used in diagnostics of the axially accelerated ion beam (Sadowski *et al* 1998, 2000, Skladnik-Sadowska *et al* 1999, 2001), as films of Thompson spectrometers (Rhee 1985), including a time resolved version (Rhee 1987, 1988). They have also been used for the detection of charged reaction products (Al-Mashhadni *et al* 1994, Todorovick 1995), and in some cases, images of the charged particle emission sources have been obtained using the *camara obscura* technique (Jäger *et al* 1985, Jäger and Herold 1987, Zakaulla 1999, Springham 2002). The way nuclear track detectors work can be summarized as follows. When a charged particle is slowed down in the detector, mainly by inelastic interactions with the plastic material, it leaves latent tracks of broken molecular bonds. These tracks can then be exposed, by attacking the plastic with some chemical agent, such as NaOH or KOH. Since the etch rate is larger over the track of broken bonds, a conical pit is produced, whose diameter depends, for a given etching time, on the charge and energy of the particle that produced it. It can be easily observed with an optical microscope. Electrochemical etching can also be used, where the etched tracks filled with the conducting etchant act as needle electrodes (Brede 1999). In this case, the electric field is amplified at the tip of the cone, and if it is high enough, electric breakdown occurs, producing an enlargement of the track. However, only chemical etching was used in this work.

The use of CR-39 ($C_{12}H_{16}O_7$) nuclear track detectors in neutron dosimetry was reviewed by Matiulla *et al* (1990). Their use as a diagnostic of neutrons from deuterium–deuterium (D–D) and deuterium–tritium (D–T) reactions has been studied by Collopy *et al* (1992), using and accelerator, and more recently by Frenje *et al* (2002), using the OMEGA laser facility. In the case of the D–D reaction, with which we are concerned in this paper, 2.45 MeV neutrons are produced, which interact with the detector mainly through elastic (n, p) scattering of protons from the detector material. Radiator foils, such as polyethylene, can be placed in front of them, in order to increase the detection efficiency. Even carbon and oxygen scattered nuclei can produce etchable tracks. For the 14.1 MeV neutrons that arise from the D–T reactions, other processes may contribute as well, such as inelastic (n, p) or (n, α) reactions with carbon or oxygen. The tracks produced by the charged particles in any of these events, allow the detection of the fusion neutrons. The efficiencies reported for D–D neutrons are $(1.3 \pm 0.4) \times 10^{-4}$ by Collopy *et al* (1992) and $(1.1 \pm 0.1) \times 10^{-4}$ by Frenje *et al* (2002). Their efficiencies for D–T neutrons are $(5.0 \pm 1.8) \times 10^{-5}$ and $(6.0 \pm 0.7) \times 10^{-5}$, respectively. Frenje *et al* (2002) have also made Monte Carlo simulations that yield consistent efficiency values.

This paper is organized as follows: in section 2 both the Fuego Nuevo II (FN-II) and PACO devices are described, as well as the experimental set-ups and procedures used in each laboratory. The analysis of the neutron angular distributions and the estimate of the total neutron yields are discussed in section 3, and conclusions are drawn in section 4.

2. The experimental set-up

The FN-II (Castillo *et al* 2002) and PACO (Castillo *et al* 1997, 2000) are two small, dense plasma focus devices; the former is located at the National Autonomous University in Mexico City, Mexico, while the latter is at the National University of the Centre of the Province of Buenos Aires, in Tandil, Argentina. They are similar in conception, but with important differences. The main relevant difference for the purpose of this work, is their inner electrode,

which is made of oxygen-free copper in FN-II, and brass in PACO. The length of both inner electrodes is 40 mm, but its diameter in PACO is 40 mm, while in FN-II it is 50 mm, matching the insulator's outer diameter. Both devices have *Pyrex* insulators, 19 mm long. In both cases the outer electrode is of the squirrel cage type, consisting of 12 bars, of 8 mm diameter and 45 mm length each, arrayed on a 100 mm diameter circle. For the shots analysed in this work the FN-II was operated at 36 kV with 4.8 kJ stored energy at the capacitor bank, while the PACO was operated at 31 kV with a stored energy of 2 kJ. The maximum currents achieved are $I_{\max} = 350$ kA and 250 kA, respectively.

There were significant differences in the procedures followed in the measurements of both devices; thus, the ones of the FN-II are described first, and then the main differences in the case of PACO are pointed out.

The neutron flux at 20° from the axis (almost head-on) and at 90° (side-on) was measured on a shot to shot basis by two silver activation counters, 54 cm away from the source. These consist of two Victoreen 1B85 Geiger–Muller counters, 10 cm long, wrapped in 500 μm silver foil, and surrounded by 6 cm of paraffin. They were calibrated with an Am–Be neutron source, and the background counts were monitored on a daily basis, in order to check the invariance of their behaviour. The counts following one minute after each shot were monitored. Within two significant figures, for the distance at which they are placed from the source, their conversion factor was found to be $(6.0\pm0.9)\times10^3$ and $(9.4\pm0.3)\times10^3$ neutrons/count str for the counters at 20° and 90° from the axis, respectively. According to the laboratory background radiation, the minimum measurable yield was found to be $(3.6\pm0.5)\times10^5$ and $(5.6\pm0.9)\times10^5$ neutrons str^{-1} for each case.

The angular distribution of the neutron flux, is measured with CR-39 polycarbonate Lantrack® chips, 1.9 cm × 0.9 cm, and 500 μm thick. The chips were arranged on a circular frame of 100 cm radius, centred at the focus, outside the discharge chamber, at nine different angles relative to the gun axis: 0°, ±45°, ±90°, ±135° and ±170°. The reason why one of the activation counters was placed at 20° from the axis, instead of putting it directly head-on, was in order to give way to the circular frame, where the plastic track detectors are placed. Suitable neutron detection was obtained covering the CR-39 with 2 mm thick polyethylene sheets. With the idea of getting a good statistical sample, the plastic detectors were exposed to several shots, such that around 90 000 counts could be accumulated on the 20° counter. This was repeated for six groups of plastic detectors, as explained in the next section.

The chemical etching of the plastic chips was performed by immersing them in KOH, 6.25 M solution, at 60 ± 1°C for 16 h. At a bulk etching rate of $V_B = 0.95\ \mu$m h^{-1}, measured according to Espinosa *et al* (1995), a 15 μm etching depth is obtained. This was deemed to be the optimum etching rate, for which the detection efficiency attained a maximum. The track density would remain constant for larger etching times. The track counting was done with an optical microscope, with a 200× magnification. A field of 0.36 mm × 0.3 mm was fixed as measurement area. A witness plastic, unexposed to the neutrons was etched along with the others, in order to subtract background tracks. Forty fields per chip were counted, in order to obtain better statistics. The optical microscope is coupled to a CCD camera and a digital image analysis system (DIAS) (Gammage *et al* 1997), allowing automatic measurements. The software used for the track counting and size analysis was Jandel Corporation Mocha® Image Analysis Software, and Microsoft Excel® for the data analysis.

The data of the PACO device, obtained a few years earlier, and partially published in Castillo *et al* (1997), were obtained with a different philosophy. Instead of following a statistical approach, the idea was to try to measure the angular distribution for a single shot. Since this is not always possible, due to the wide difference in the neutron yield from shot to shot, the detectors were exposed for only a few shots, as is further discussed in the next section. On the

other hand, bare CR-39 detectors were used, without a polyethylene cover, as opposed to the case of the FN-II experiments. Further studies by the FN-II group have shown, however, that there is no significant difference, when detecting D–D neutrons, as previously found by Collopy *et al* (2002). The angles at which they were placed were 0°, ±5°, ±10°, ±16, ±25° and ± 90°. The fact that there was no measurement at backward angles was not important for PACO, although it would have been important in the FN-II, as will be seen in the analysis of the results. The procedure for etching the plastics was the same in both devices, but in PACO the track counting was not automatic, and there was no size analysis. Activation counters, similar to those used in the FN-II device were placed at the same angles. However, their efficiency was lower, so the conversion factor was 4.4×10^4 neutrons per count str for both counters.

3. Analysis and discussion of experimental results

As in the previous section, we proceed by discussing first the experimental results in the FN-II. Six groups of shots are analysed in this work. Three of them, which we shall call FN-II(a)–(c), were done on pure deuterium, at 2.7 ± 0.1 Torr, where the device is optimized for neutron emission, as described in Castillo *et al* (2002). Three more were obtained with deuterium–argon admixtures: group FN-II(d) was produced with an admixture of 0.031 Torr of argon, and the rest, up to 2.751 Torr of deuterium. The corresponding ratios of argon to total pressure were 0.061/2.750 for group FN-II(e) and 0.275/2.775 for group FN-II(f). In the case of PACO, three shorter groups (a)–(c) of shots were considered for the present analysis, with a filling pressure of pure deuterium at 1.1 ± 0.1 Torr, as described in Castillo (1997). The number of counts obtained for 60 s after each shot, were recorded for both silver activation detectors. The description of the groups of shots considered in this work is given in table 1. Since a few shots, particularly the first ones for a fresh gas charge, do not always produce neutrons, only those that yield a neutron count clearly above the background are considered. Thus, both the logbook shot numbers and the number of shots (NS) actually considered for the analysis are given. The difference in the approach when collecting the data in both devices is clearly seen. While in the FN-II the main idea was to get a statistical sample, in PACO the idea was to get an angular distribution as close as possible to that produced by a single shot. It may be added that the oxygen-free copper electrode and the geometry used in the former helps to get a better

Table 1. Description of the groups of shots analysed in this work. The logbook shot numbers are shown in the second column, while the total number of shots, for which the activation counters clearly showed neutron production (NS), is given in the third column. NC_{20} and NC_{90} are the total number of counts accumulated on the counters at 20° and 90°, respectively, for the whole group, while N_{20} and N_{90} are the average number of counts per shot and the standard deviation for each case. Since there are only a few shots in PACO, the difference between the average and the farthest value is taken instead of the standard deviation.

	Shot numbers	NS	NC_{20}	NC_{90}	N_{20}	N_{90}
FN-II(a)	4316–4361	42	91 532	56 935	2149 ± 1060	1356 ± 644
FN-II(b)	4962–5030	57	106 337	54 229	1857 ± 1417	944 ± 497
FN-II(c)	5262–5351	60	102 305	66 496	1693 ± 1193	1095 ± 612
FN-II(d)	5171–5195	24	85 718	45 222	3572 ± 1756	1884 ± 748
FN-II(e)	5208–5242	33	90 598	49 590	2745 ± 1089	1503 ± 446
FN-II(f)	5102–5165	54	68 648	44 983	1207 ± 700	785 ± 334
PACO(a)	6550–6559	2	577	393	288 ± 198	196 ± 129
PACO(b)	7306–7311	3	1 090	912	363 ± 214	304 ± 141
PACO(c)	7312–7325	4	361	301	90 ± 78	75 ± 68

frequency of 'good shots'. The total number of accumulated counts was an important criterion in the FN-II to determine whether the plastic track detectors were ready for analysis. Also shown in table 1 are the averages and standard deviations of the counts for each group. Since the data for PACO are too few for a statistical analysis, the difference between the average and the farthest value is reported, instead of the standard deviation.

The track density for each chip of plastic detector was measured as described above, and the angular distribution, normalized to the maximum yield on-axis was plotted. For all the groups obtained from pure deuterium as a filling gas, the data could be adjusted by a Gaussian function of the angle θ superposed on a pedestal:

$$f(\theta) = B + g(\theta), \tag{1}$$

where B is a constant and

$$g(\theta) = \left(\frac{C}{\sigma\sqrt{2\pi}}\right) \exp\left(-\frac{\theta^2}{2\sigma^2}\right). \tag{2}$$

The values of the parameters B, C and σ, for each group of shots can be obtained by using the Origin® software. Figures 1 and 2 show the plots for each case in both devices. Thus, there are clearly isotropic, A_1, and anisotropic, A_2, contributions, which most probably originate from different neutron generation mechanisms. They can be obtained by integrating, respectively, the first and second terms of (1) over the solid angle:

$$A = 4\pi B + 2\pi \int_0^{\pi} g(\theta) \sin\theta \, \mathrm{d}\theta = A_1 + A_2, \tag{3}$$

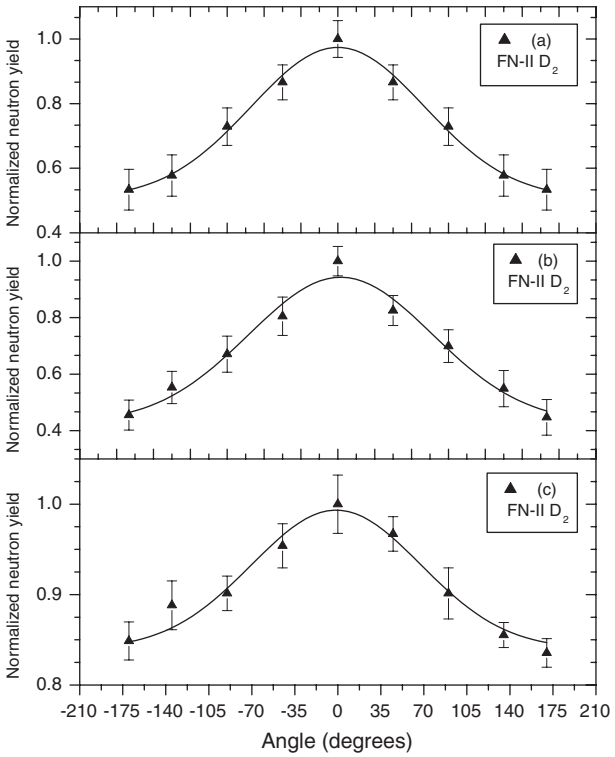


Figure 1. Plots for the angular distributions of the neutron emissions of the FN-II device, for groups of detectors (a)–(c), when pure deuterium is used as filling gas.

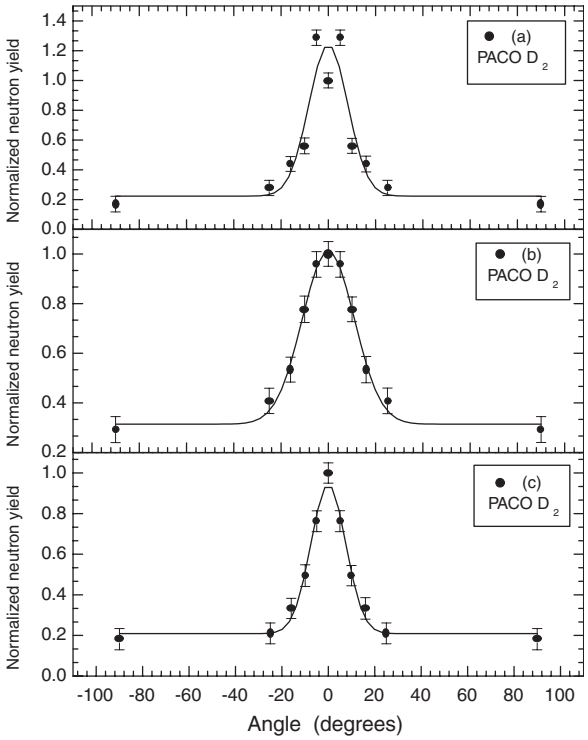


Figure 2. Plots for the angular distributions of the neutron emissions of the PACO device, for groups of detectors (a)–(c), when pure deuterium is used as filling gas.

Table 2. Isotropic A_1 and anisotropic A_2 components of each group of shots, according to equations (3) and (4). Ratios $\alpha_0 = f(0^\circ)/f(90^\circ)$ and $\alpha_{20} = f(20^\circ)/f(90^\circ)$ obtained from the fits to the angular distributions, and the experimental ratio $\alpha_c = N_{20}/N_{90}$ obtained from the activation counters. When obtaining the latter, α_{20} was computed for each shot, rather than taking the values given in table 1, and corrections have been made to account for the difference in efficiencies between the counters, where it was needed. Partial neutron yield for both the isotropic, Y_{Iso}, and anisotropic Y_{Aniso} contributions, as well as the total one are given. They are obtained from a scaling factor S, which is the average of S_{20} and S_{90}, as discussed in the text.

	A_1	A_2	α_0	α_{20}	α_c	S $\times 10^7$	Y_{Iso} $\times 10^8$	Y_{Aniso} $\times 10^7$	Y_{Total} $\times 10^8$
FN-II(a)	6.37	2.78	1.36	1.34	1.20 ± 0.18	1.95 ± 1.20	1.24 ± 0.76	5.42 ± 3.34	1.78 ± 1.09
FN-II(b)	5.38	3.26	1.41	1.37	1.38 ± 0.34	1.26 ± 0.95	0.68 ± 0.53	4.11 ± 3.19	1.09 ± 0.85
FN-II(c)	10.56	0.88	1.10	1.09	1.12 ± 0.21	1.09 ± 0.78	1.15 ± 0.83	0.96 ± 0.68	1.25 ± 0.90
FN-II(d)	7.05	3.45	1.11	1.11	1.41 ± 0.23	2.17 ± 1.20	1.53 ± 0.85	7.48 ± 4.14	2.28 ± 1.26
FN-II(e)	5.76	3.88	1.13	1.13	1.37 ± 0.21	1.82 ± 0.77	1.05 ± 0.45	7.06 ± 2.96	1.76 ± 0.75
FN-II(f)	6.44	4.13	1.12	1.12	1.13 ± 0.21	0.80 ± 0.49	0.52 ± 0.31	3.31 ± 2.02	0.85 ± 0.51
PACO(a)	2.81	0.13	5.53	1.24	1.43 ± 0.09	4.25 ± 3.54	1.19 ± 0.99	0.55 ± 0.51	1.26 ± 1.04
PACO(b)	3.95	0.16	3.22	1.43	1.21 ± 0.21	3.94 ± 2.47	1.56 ± 0.97	0.63 ± 0.39	1.62 ± 1.01
PACO(c)	2.63	0.08	4.51	1.10	1.22 ± 0.05	1.69 ± 1.57	0.44 ± 0.42	0.13 ± 0.12	0.45 ± 0.43

where the second term is computed by numerical integration. The corresponding contributions for each case are given in table 2.

It is most significant that in the data obtained form PACO, the Gaussian distribution is highly peaked in comparison with the results obtained form FN-II. Since it falls quickly, the

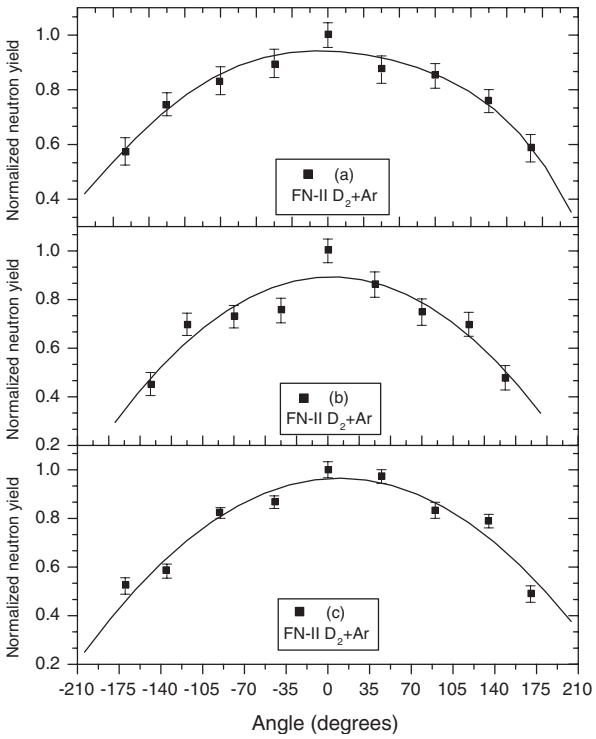


Figure 3. Plots for the angular distributions of the neutron emissions of the FN-II device, for groups of detectors (d)–(f), when a deuterium–argon admixture is used as filling gas.

fact that no plastics were placed at backward angles is irrelevant to the analysis. However, the anisotropic contribution is generally higher in the case of FN-II. It must be noted that the case PACO(a) shows a bimodal, symmetric distribution, rather than a simple fit of the form (2). This hollow distribution is consistent with results reported elsewhere (Sadowski *et al* 1998), where it has been shown that the accelerated deuteron beam is conical for some PACO shots.

When the data obtained from the deuterium–argon admixture are plotted, the Gaussian does not fall fast enough at large angles to allow a clear separation of the isotropic and anisotropic components, since the area under the Gaussian is larger than the actual anisotropic component. A parabola, $f(\theta) = B_0 + B_1\theta + B_2\theta^2$, is chosen in this case, as may be seen in figure 3, since it allows a more straightforward measurement of each component. In this case

$$A_1 = 4\pi f(180^\circ) \qquad \text{and} \qquad A_2 = 2\pi \int_0^\pi f(\theta) \sin\theta \, \mathrm{d}\theta - A_1. \tag{4}$$

The corresponding isotropic and anisotropic contributions for these cases are shown in table 2 as well.

Anisotropy is often given as the ratio of the fluxes measured by a detector or activation counter head-on and another one side-on. If the angular distribution is highly peaked, such as is found to be the case in PACO, this ratio will be extremely high, in spite of the fact that its anisotropic contribution is actually small. Table 2 shows a comparison, using the values obtained from (1) (with the necessary modifications for cases FN-II(d)–(f)), of the ratios $\alpha_0 = f(0^\circ)/f(90^\circ)$ and $\alpha_{20} = f(20^\circ)/f(90^\circ)$ for each case. As can be seen, for distributions such as those obtained in PACO, the former can be substantially greater than the latter. The highly peaked distributions observed here may be the explanation for the apparently high values

of anisotropy previously reported by the PACO team. The origin of this unique result is still to be determined. Then, it is also important to compare α_{20} with the ratio $\alpha_c = N_{20}/N_{90}$ obtained experimentally from the activation counters. The values given in table 2 are calculated from the ratios obtained from each shot, taking into account the difference in the efficiencies of the counters, where necessary, rather than from the values of N_{20} and N_{90} given in table 1. As can be seen, there is a reasonable agreement between α_{20} and α_c.

In order to find the absolute value of neutrons for each contribution, a scaling factor for the angular distribution can be found, comparing the silver activation counters data close to the axis and side-on, with the values $f(20^\circ)$ and $f(90^\circ)$, respectively. From the counters and their calibration conversion factors, the fluxes for both positions, $E(20^\circ) = \mathrm{d}Y/\mathrm{d}\Omega|_{20^\circ}$ and $E(90^\circ) = \mathrm{d}Y/\mathrm{d}\Omega|_{90^\circ}$ are obtained, where E is given in neutrons str^{-1}. Then, we get two scaling factors: $S_{20^\circ} = E(20^\circ)/f(20^\circ)$ and $S_{90^\circ} = E(90^\circ)/f(90^\circ)$, which are slightly different, but consistent within experimental error. The average scaling factor S can then be used, multiplying it by the isotropic A_1 and anisotropic A_2 components, respectively, in order to get the corresponding contributions to the neutron yield. These results are shown in table 2, along with the total neutron yield.

When obtaining the track density by means of the DIAS, in the FN-II analysis, only tracks with ratio of minor axis to major axis that were greater than 0.9 were considered, and the distribution of their average diameter was obtained. The full set of chips for each group was considered for this measurement. The histogram shown in figure 4(*a*) depicts the diameter distribution of the tracks per mm^2, for the case of FN-II(c), which is typical of the shots where the filling gas is pure deuterium. Two peaks can be seen: 78% of the tracks fall within a strongly peaked Gaussian distribution centred around 19.7 μm, with a full width at half maximum (FWHM) of 2.7 μm. The remaining 22% fall in a second clearly defined peak centred at 9.7 μm with a FWHM of 1.9 μm. The larger tracks are presumably produced by protons kicked off the polyethylene plate by elastic (n, p) scattering. The fact that the distribution is so narrow is an effect of considering a large ratio of minor to major radii in the track diameter, and a strong indication that the neutrons that are being detected are strongly mono-energetic. The tracks in the smaller peak are attributable to the knock off of larger nuclei. The results are found to be slightly different for the size of the tracks produced when a deuterium–argon admixture is used. Figure 4(*b*) shows one such case (FN-II(d)). As in the case where pure deuterium is used, the histogram shows two peaks again. However, the larger peak is broader, and cannot be properly fitted by a Gaussian. If one forces a Gaussian fit to it, the maximum is found to be at 16.4 μm, with a FWHM of 5.9 μm. The smaller peak is comparable with the one obtained for pure deuterium. Its maximum stands at 9.8 μm, with a FWHM of 2.3 μm.

An important issue remains to be clarified regarding the neutron diagnostics using the CR-39 plastic track detectors: according to both Collopy *et al* (1992) and Frenje *et al* (2002), their efficiency for D–D neutron detection is $\sim 10^{-4}$. For the purpose of order of magnitude estimation, if we assume our neutron yield to be isotropic, around 10^8 neutrons per shot, according to our results, then 1 m away from the focus the neutron flux should be around 10^3 neutrons cm^{-2}. This means 10^{-1} tracks cm^{-2} per shot should be produced in our experiments. In the the PACO device, where few shots are accumulated (one can assume essentially one shot per case studied, since not all of them show a significant neutron production, as can be seen in table 1), the track density is ~ 10 tracks cm^{-2}. In the FN-II measurements, several tens of shots are accumulated, and the track density, with 15.2 μm etch depth, is $\sim 10^2$ tracks cm^{-2}. Thus, the efficiency we are obtaining is $\sim 10^{-2}$, two orders of magnitude greater than those of Collopy *et al* and Frenje *et al*. The etch depth, cannot be responsible for this. Although the one reported by Frenje *et al* (12 μm) is slightly smaller than ours, the

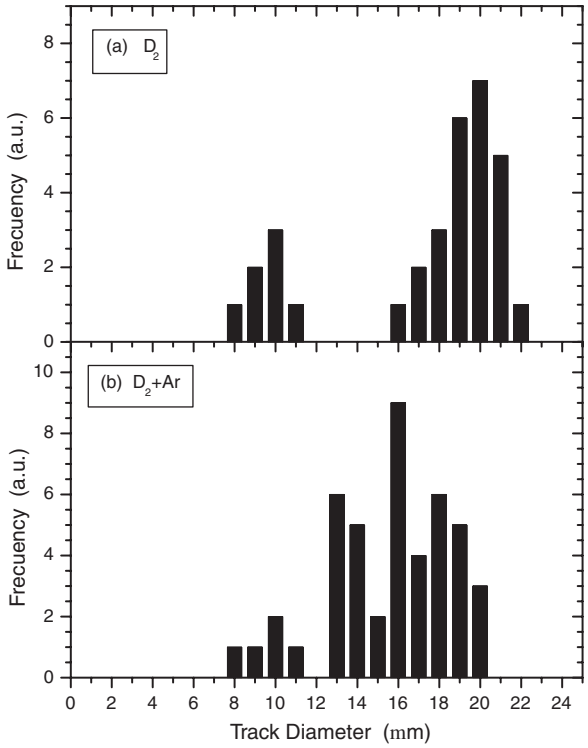


Figure 4. Histograms of the track sizes: (*a*) group of shots FN-II(c), when pure deuterium is used; (*b*) group FN-II(d), when an admixture of deuterium and argon is used. Only those tracks with ratio of minor axis to major axis that were greater than 0.9 were considered.

difference in the efficiency we find from our own measurements is no larger than a factor of 1.3. We have also checked that, at least for D–D neutrons, there is no significant difference in the efficiency observed when a polyethylene sheet is placed over the CR-39. What can be asserted from the measurements we carried out several times is that, although the efficiency we observe is clearly at odds with the ones previously reported, the results presented in this paper are clearly reproducible.

It can be suspected that the paraffin of the silver activation counter placed close to the axis may be moderating some of the neutrons, increasing the detection efficiency on-axis, and thus modifying the angular distribution. In order to find out if this is the case, the counter was removed in the FN-II experiments, and the same qualitative results were obtained.

4. Conclusions

An extensive study of the angular distributions of neutron emissions has been carried out, for two similar, but yet different plasma focus devices, using CR-39 plastic nuclear track detectors. It has been found that, when pure deuterium is used as a filling gas, the distributions can be generally fitted by a Gaussian function superposed on a pedestal. In some rare cases, such as the one of case PACO(a), the distribution may be bimodal. However, the peak is narrow enough to allow the kind of analysis proposed in this work. This reveals the coexistence of two neutron generation mechanisms; one that produces an isotropic component, and one that produces an anisotropic component in the neutron emission. The latter is usually smaller than

the former, and ranges from 4% to 38% of the total yield. However, the most interesting feature is that in the PACO device this anisotropic component is extremely peaked. If the usual way of reporting anisotropy, as the ratio of the fluxes head-on and side-on were used, the result might be extremely misleading, since it could be very large, even when the anisotropic contribution could actually be rather small. Furthermore, the lesson is that caution should be taken not to use the readings of counters placed head-on in order to get the total neutron yield, for this may result in gross overestimation. Aware of this, most groups base their total yield estimation on counters placed side-on. Since the details of the angular distribution can change with the filling gas and the special features of each device, it is advisable, when estimating the total neutron yield, whenever possible, to get the characteristic angular distribution of a device, using techniques of the sort described in this work. For major devices in the megajoule range, where the neutron yield is $>10^{11}$, single shot angular distributions should be easily produced. This is clearly backed by the use of CR-39 in neutron diagnostics of major inertial confinement fusion experiments, such as the OMEGA (Frenje *et al* 2202), whose neutron yield is approximately the same.

The angular distributions obtained when deuterium and argon admixtures were used, are apparently inconsistent with earlier observations by Aliaga and Choi (1998), who observe a decrease in the time emission of neutrons side-on, using time resolved diagnostics. This should translate into an increase in the anisotropy, rather than a smoothing of it, as observed in this work. Further research with time resolved diagnostics is needed to clarify this. It is also interesting to note that the diameter distribution of the tracks produced by the kicked-off protons is not as well defined when an admixture is used, indicating that there might be a slight spread in their energy.

It has become clear that an automatic measurement system, both for track counting and size analysis, such as the DIAS described here is desirable, if nuclear track detectors are to be of practical use.

For the purpose of applications of the plasma focus, and especially for the smaller size versions under design at several laboratories, it is important to know its statistical behaviour. This is something that still depends largely on design features, such as the material and geometry of the inner electrode. Thus, it has been observed that a more consistent behaviour is obtained with the electrode used in this work with the FN-II, than with that of PACO. This had been previously demonstrated comparing two different oxygen-free copper electrodes in Castillo (2002). However, the neutron yield still varies widely from shot to shot, as can be seen in the standard deviations shown in table 1. Improvement in this direction is clearly desirable.

Last but not least, it is to be noted that the efficiency observed in this work for D–D neutron detection by CR-39 ($\sim 10^{-2}$), is roughly two orders of magnitude greater than that reported in earlier studies. Although this is still to be clarified through further investigation, the results presented in this paper were validated by careful repetition of the experiment and track counting in the FN-II device.

Acknowledgments

This work was partially supported by the DGAPA-UNAM grant IN105100 and CONACYT grant 27974-E.

References

Aliaga-Rossel R and Choi P 1998 *IEEE Trans. Plasma Sci.* **26** 1138
Al-Mashhadani E M, Sadowski M and Szydlowski A 1994 *Plasma Phys. Reports* **20** 180

Bernard A *et al* 1998 *Moscow Phys. Soc.* **8** 93
Bernstein M J and Hai F 1970 *Phys. Lett.* A **31** 317
Brede H J, Gisbertz A, Kohler I, Pitt E and Scharmann A 1999 *Radiat. Prot. Dosim.* **85** 113
Brzosko J S, Degnan J H, Filippov N V, Freeman B L, Kiutlu G F and Mather J W 1997 Comments on the feasibility of achieving scientific break-even with a plasma focus machine *Current Trends in International Fusion Research* ed E Panarella (New York: Plenum) pp 11–32
Castillo F, Milanese M, Moroso R and Pouzo J 1997 *J. Phys. D: Appl. Phys.* **30** 1499
Castillo F, Milanese M, Moroso R and Pouzo J 2000 *J. Phys. D: Appl. Phys.* **33** 141
Castillo F, Herrera J J E, Rangel J, Alfaro A, Maza M A, Sakaguchi V, Espinosa G and Golzarri J I 2002 *Brazilian J. Phys.* **32** 3
Collopy M T *et al* 1992 *Rev. Sci. Instrum.* **63** 4892
Dubrovsky A V, Gribkov V A, Kozlova T A, Volobuev L V and Orlova M A 1998 *J. Tech. Phys.* **39** (Special Suppl) 133
Espinosa G, Gammage R B, Meyer K, Heeler R B and Salasky M 1995 *Radiat. Prot. Dosim.* **59** 227
Frenje J A *et al* 2002 *Rev. Sci. Instrum.* **73** 2597
Gammage R B and Espinosa G 1997 *Radiat. Meas.* **28** 835
Herold H *et al* 1985 Two phases of neutron production in the Poseidon plasma focus *Proc. 10th IAEA Conf. on Plasma Physics and Controlled Fusion (London, 1984)* vol II (Vienna: IAEA) pp 579–89
Jäger U, Bertalot L and Herold H 1985 *Rev. Sci. Instum.* **56** 77
Jäger U and Herold H 1987 *Nucl. Fusion* **27** 407
Kelly H and Márquez A 1996 *Plasma Phys. Control. Fusion* **38** 1931
Lee S, Lee P, Zhang G, Feng X, Gribkov VA, Liu M, Serban A and Wong TK 1998 *IEEE Trans. Plasma Sci.* **26** 1119
Maisonnier Ch, Pecorella F, Rager J P and Samuelli M 1972 Recent progress in research on plasma focus *Proc. 5th Eur. Conf. Plasma Phys. Controlled Fusion (Grenoble, France)* vol 2, p 183
Mather J W 1971 *Dense Plasma Focus Methods in Experimental Physics* vol 9, ed R H Lovberg and H R Griem (New York: Academic) pp 187–249
Matiullah N, Ahmad S A, Durrani and Khan G A 1990 *Nucl. Instrum. Methods* B **51** 76
Moo S P, Chakrabarty C K and Lee S 1991 *IEEE Trans. Plasma Sci.* **19** 515
Moreno C, Vénere M, Barbuzza R, del Fresno M, Ramos R, Bruzzone H, Florido P J, González P J and Clausse A 2002 *Brazilian J. Phys.* **32** 20
Milanese M and Pouzo J 1978 *Nucl. Fusion* **18** 533
Muhling E, Schumacher U and Paretzke M G 1984 *Nucl. Tracks* **9** 113
Rhee M J 1985 *Rev. Sci. Instrum.* **55** 1229
Rhee M J, Schneider R F and Weidman D J 1987 *Sci. Instrum.* **58** 240
Rhee M J, Schneider R F and Weidman D J 1988 *Phys. Fluids* **31** 703
Sadowski M, Skladnik-Sadowska E, Baranowski J, Milanese M M, Moroso R and Pouzo J 1998 *J. Tech. Phys.* **39** (Special Suppl) 109
Skladnik-Sadowska E, Baronowski J, Milanese M M, Moroso R, Pouzo J, Sadowski M and Zewroski J 1999 *J. Tech. Phys.* **40** 129
Sadowski M, Skladnik-Sadowska E, Baranowski J, Zebrowski J, Kelly H, Lepone A, Márquez M, Milanese M, Moroso R and Pouzo J 2000 *Nukleonica* **45** 179
Skladnik-Sadowska E, Baronowski J, Milanese M M, Moroso R, Pouzo J, Sadowski M and Zewroski J 2001 *Radiat. Meas.* **34** 315
Springham S V, Lee S and Moo S P 2002 *Brazilian J. Phys.* **32** 172
Todorovick Z, Antanasijevic R, Sevic D, Zaric A, Konjevic D J, Vukovic J, Puric J and Cuk M 1995 *Radiat. Meas.* **25** 265
Yap S I, Moo S P, Wong C S, Choi P and Dumitrescu-Zoita C 1997 *Proc. 4th Int. Conf. on Dense Z-Pinches (Vancouver, Canada) (AIP Conf. Proc.)* vol 409 (Woodbury: AIP) pp 75–8
Zakaullah M, Akhtar I, Murtaza G and Waheed A 1999 *Phys. Plasmas* **6** 3188s